RESEARCH ARTICLE

Seasonal dynamics of the marine CO_2 system in Adventfjorden, a west Spitsbergen fjord

Ylva Ericson[1,2], Melissa Chierici[1,3], Eva Falck[1,2], Agneta Fransson[4], Elizabeth Jones[3] & Svein Kristiansen[5]

[1]Department of Arctic Geophysics, University Centre in Svalbard, Longyearbyen, Norway;
[2]Geophysical Institute, University of Bergen, Bergen, Norway;
[3]Institute of Marine Research, Fram Centre, Tromsø, Norway;
[4]Norwegian Polar Institute, Fram Centre, Tromsø, Norway;
[5]Department of Arctic and Marine Biology, UiT—The Arctic University of Norway, Tromsø, Norway

Abstract

Time series of the marine CO_2 system and related parameters at the IsA Station, by Adventfjorden, Svalbard, were investigated between March 2015 and November 2017. The physical and biogeochemical processes that govern changes in total alkalinity (TA), total dissolved inorganic carbon (DIC) and the saturation state of the calcium carbonate mineral aragonite (Ω_{Ar}) were assessed on a monthly timescale. The major driver for TA and DIC was changes in salinity, caused by river runoff, mixing and advection. This accounted for 77 and 45%, respectively, of the overall variability. It contributed minimally to the variability in Ω_{Ar} (5%); instead, biological activity was responsible for 60% of the monthly variations. For DIC, the biological activity was also important, contributing 44%. The monthly effect of air–sea CO_2 fluxes accounted for 11 and 15% of the total changes in DIC and Ω_{Ar}, respectively. Net community production (NCP) during the productive season ranged between 65 and 85 g C m^{-2}, depending on the year and the presence of either Arctic water or transformed Atlantic water (TAW). The annual NCP as estimated from DIC consumption was 34 g C m^{-2} yr^{-1} in 2016, which was opposite in direction but similar in magnitude to the integrated annual air–sea CO_2 flux (i.e., uptake of carbon from the atmosphere) of −29 g C m^{-2} yr^{-1} for the same year. The results showed that increased intrusions of TAW into Adventfjorden in the future could possibly lower the NCP, with the potential to reduce the CO_2 buffer capacity and Ω_{Ar} over the summer season.

Keywords

Marine carbonate system; aragonite; net community production; Arctic fjord biogeochemistry; Svalbard

Correspondence

Ylva Ericson, Department of Arctic Geophysics, University Centre in Svalbard, PO Box 156, NO-9171 Longyearbyen, Norway. E-mail: ylva.ericson@unis.no

Abbreviations

ArW: Arctic water; AW: Atlantic water; CC: coastal current; CTD: conductivity–temperature–depth instrument; DIC: total dissolved inorganic carbon; NCP: net community production; pCO_2: partial pressure of CO_2; S: salinity; T: temperature; TAW: Transformed Atlantic Water; TA: total alkalinity; UNIS: University Centre in Svalbard; WSC: West Spitsbergen Current; Ω_{Ar}: saturation state of aragonite

Introduction

The Svalbard region has changed dramatically over the last couple of decades. The annual mean air surface temperature at Svalbard Airport, western Spitsbergen, increased by 4°C between 1970 and 2012 (Nordli et al. 2014). Onarheim et al. (2014) showed, using the ERA-Interim reanalysis product from the European Centre for Medium-Range Weather Forecasts, that the warming north of Svalbard was especially pronounced in the winter season where the mean air temperature has increased by nearly 7°C since 1979. Meanwhile, the AW of the northward flowing WSC has warmed by 0.3°C per decade, which has resulted in reduced sea-ice cover north of the archipelago (Onarheim et al. 2014). AW in the west Spitsbergen fjords has also become warmer (0.2°C/decade in Isfjorden [Pavlov et al. 2013]), and more frequent intrusions of AW into the western fjord systems are likely the cause of the observed decrease in sea-ice cover in this region (Isaksen et al. 2016; Muckenhuber et al. 2016). Following the observed warming, a retreat of glaciers in Spitsbergen has taken place (e.g., Ziaja 2005; Ewertowski 2014; Grabiec et al. 2017; Marlin et al. 2017), resulting in increased glacial meltwater being released to the surrounding coastal surface waters. Observations of permafrost thawing also suggest that this High-Arctic environment is in transition and especially vulnerable to future climate change (Sobota & Nowak 2014).

Citation: *Polar Research* 2019, *38*, 3345, http://dx.doi.org/10.33265/polar.v38.3345

The question is how the west Spitsbergen fjords will respond to these changes, both in terms of their potential to take up carbon dioxide (CO_2) from the atmosphere, which is largely related to the biological production that drives the surface water pCO_2 variability (e.g., Fransson et al. 2016; Ericson et al. 2018), and in terms of their geochemical resistance to ongoing ocean acidification (e.g., Fransson et al. 2015). Ocean acidification refers to the shift in the marine CO_2 system towards a lower pH and less carbonate ions (CO_3^{2-}), which results from the uptake of anthropogenic CO_2 (e.g., Doney et al. 2009). The CO_3^{2-} concentration $[CO_3^{2-}]$ determines the calcium carbonate ($CaCO_3$) saturation state of seawater (Ω) through its proportional relationship

$$\Omega = \frac{\left[CO_3^{2-}\right]\left[Ca^{2+}\right]}{K_{sp}^{*}}, \quad (1)$$

where K_{sp}* is the stoichiometric solubility product, that is, the product of the calcium ion concentration $[Ca^{2+}]$ and $[CO_3^{2-}]$ of seawater that is saturated with $CaCO_3$. Changes in $[CO_3^{2-}]$ thus directly affect the $CaCO_3$ solubility and saturation state, which has consequences for calcifying marine organisms. For that reason, Ω is a commonly used indicator of ocean acidification. In terms of the global surface ocean, the $[CO_3^{2-}]$ can be approximated to the difference between TA and DIC with an uncertainty in the order of 10% (Sarmiento & Gruber 2006). This uncertainty is probably larger for coastal waters. Changes in TA and DIC, driven by physical and biogeochemical processes, will also result in a change in $[CO_3^{2-}]$ and hence Ω, which has implications for progressing ocean acidification.

This study shows one of the first time series with a monthly resolution of the marine CO_2 system (measured TA and pH, calculated DIC, pCO_2, $[CO_3^{2-}]$, Ω of the calcium carbonate mineral aragonite and the Revelle factor) in a Spitsbergen fjord—Adventfjorden (Fig. 1)—over a 32-month period between 2015 and 2017. The seasonal variability of these chemical properties is presented together with water column T, S, and the concentrations of nitrate $[NO_3^-]$ and silicic acid $[Si(OH)_4]$. The physical and biogeochemical processes that control the monthly variability in TA, DIC and Ω_{Ar} were investigated, which will give some insight on the sensitivity of the water column to ocean acidification. NCP, based on monthly changes in DIC and $[NO_3^-]$, is also presented, because this can be a major control of the marine CO_2 system. The effect of the presence of different water masses at the IsA Station on the CO_2 system is discussed at the end.

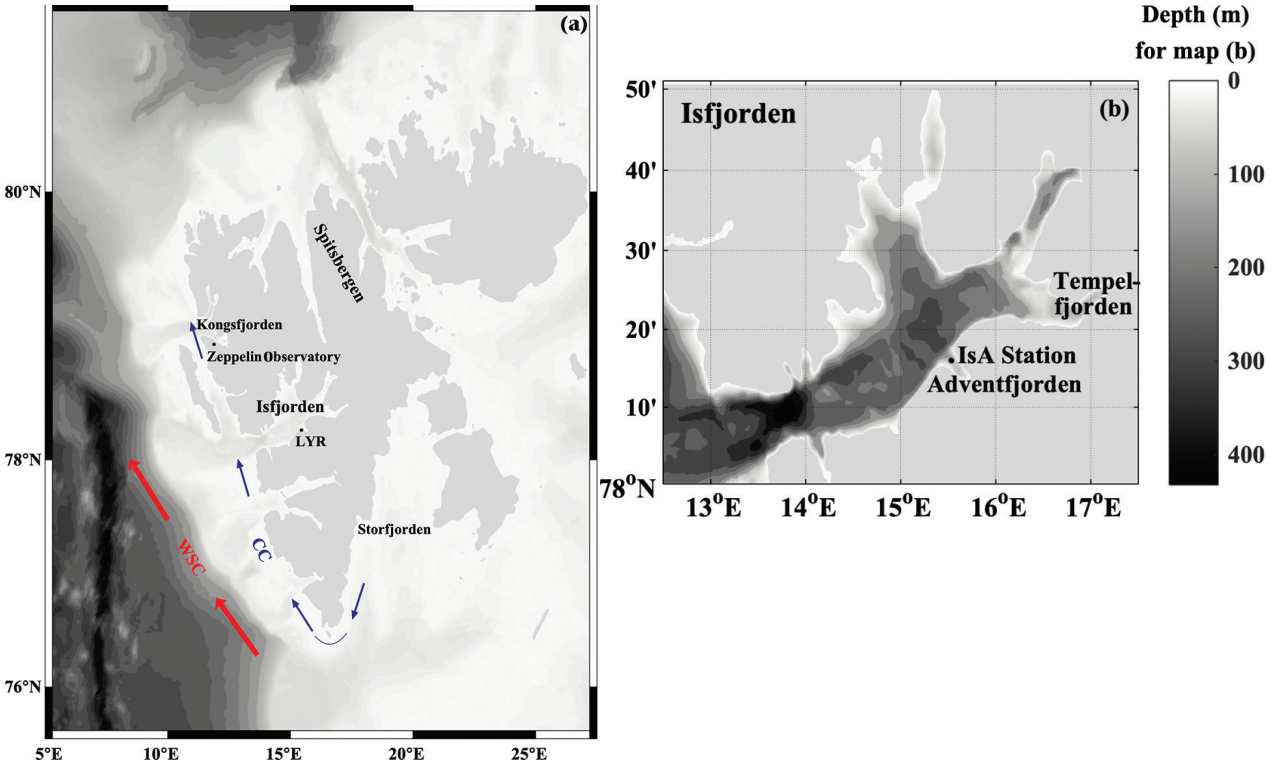

Fig. 1 (a) Map Spitsbergen, the main island in the Svalbard Archipelago, and the surrounding shelf with the locations of Isfjorden, including Svalbard Airport (LYR), close to the opening of Adventfjorden, and the Zeppelin Observatory in Ny-Ålesund, in the vicinity of Kongsfjorden. The CC and the WSC are depicted with blue and red arrows, respectively. (b) Map of Isfjorden showing the locations of Adventfjorden and the IsA Station (N 78°16.0, E 15°32.0, black dot).

Citation: *Polar Research* 2019, *38*, 3345, http://dx.doi.org/10.33265/polar.v38.3345

Study area

Beginning in March 2015 and continuing until November 2017, fieldwork took place at the IsA Station (Fig. 1b), located at 78°16.0 N, 15°32.0 E, with a bottom depth of 95 m and maximum sampling depths with a mean value of 81 ± 8 m. The sampling depths varied depending on the vessel and equipment being used. The station is in the outer part of Adventfjorden, a small branch of the larger Isfjorden system, on the west Spitsbergen coast. Two external source waters influence the fjords in this region. Firstly, relatively cold ArW (S < 34.7) that originates in the Barents Sea (e.g., Cottier et al. 2005; Nilsen et al. 2008) is transported with the northerly CC (Fig. 1a). Secondly, warmer and more saline AW (S > 34.9) flows northwards with the WSC (Fig. 1a) off the continental shelf, which, given the right atmospheric forcing, can be projected onto the shelf and occasionally into the fjords (e.g., Cottier et al. 2005; Nilsen et al. 2008; Nilsen et al. 2016). AW is to some extent mixed with ArW on the shelf, and as such, it is typically referred to as TAW (34.7 < S < 34.9) when it enters the fjords. The water masses are generally topographically steered inside Isfjorden and circulate counter-clockwise around the fjord boundaries.

Glacial melt is probably the most important freshwater source to the Isfjorden system (Nilsen et al. 2008). The surrounding watershed of Adventfjorden brings a combination of snow and glacial runoff that reaches peak discharge during the summer season. This water has rather low concentrations of TA and DIC. Measured and calculated values of 294 ± 3 and 339 ± 7 µmol kg^{-1} for TA and DIC, respectively, were observed in the Adventdalen (Advent valley) riverbed in 2015 (Ericson et al. 2018). During the study period, sea ice was scarce in Isfjorden and typically non-existent at the IsA Station, where the water temperature remained above freezing.

Data and methods

Analytical methods

Data were collected at least once every month or more frequently, except for January and September 2017 when data are missing. Sampling started with in situ measurements of T and S. Different CTD profilers (SAIV A/S SD204 CTD, Sea-Bird SBE9/SBE37/SBE19+) were used on different occasions, but from the beginning of 2016, the SBE19+, which was calibrated each year, was the principal device. This instrument was also deployed together with either the SBE37 or the SD204 to cross-check the sensors on a couple of occasions. The salinity data from the SD204 were higher by 0.1 in 2016 and 2017, and this offset was corrected for (in total five sampling occasions). CTD measurements failed on two occasions: on 22 April 2015 (CTD data from 17 April 2015 were used instead, assuming no significant changes over the five days) and on 7 November 2017. (Salinity was measured with a Portasal 8410A salinometer and calibrated against the International Association for the Physical Sciences of the Oceans standard seawater from OSIL Environmental Instruments and Systems. The temperature data were obtained from 24 October 2017.) Also, the pressure sensor used on 20 September 2016 performed poorly, and the pressure was modelled to fit the few reasonable measurements from the sensor with the salinity subsequently recalculated for the new pressure.

Seawater samples for pH, TA and nutrients, $[NO_3^-]$ and $[Si(OH)_4]$, were drawn from a Niskin bottle following standard procedures (Dickson et al. 2007). The pH/TA samples were collected in 250 mL borosilicate glass bottles and were typically analysed the day after or sooner at UNIS in Longyearbyen, Norway, except for samples collected on 29 April 2015 and 13 September 2016, which were analysed two days later, and samples collected on 29 August 2015, which were preserved with mercuric chloride and analysed within six weeks. The nutrient samples were kept in dark, stored frozen in 125 mL Nalgene® bottles and analysed within a year.

A non-purged open cell potentiometric method (Metrohm© Titrando system, Switzerland), with a non-linear least square optimization (Dickson & Goyet 1994), was used to determine TA. The precision, as estimated from the mean of the absolute values of the differences between duplicate analyses, was ± 2.3 µmol kg^{-1}. Although the method assumes no air–sample gas exchange, the impact this has on the calculation is small and negligible when the samples are compared against Certified Reference Materials (purchased from A. Dickson, Scripps Institution of Oceanography, USA). The Certified Reference Materials TA values have a standard deviation <1 µmol kg^{-1} and the systematic uncertainty will thus be in the same order as the precision. Spectrophotometric measurements of seawater samples, using a diode-array spectrophotometer and the unpurified indicator dye metacresol purple, determined pH on the total hydrogen scale, according to Clayton & Byrne (1993). The impact of the indicator dye on the pH of the samples was corrected for according to Chierici et al. (1999). The precision was ± 0.001. The laboratory took part in a CO_2 inter-laboratory comparison arranged by the laboratory of A. Dickson (Scripps Institution of Oceanography) in May 2017. The measured TA from the UNIS laboratory was <1 µmol kg^{-1} from the certified TA of the CO_2 Inter-laboratory comparison samples. For the unknown sample with ambient pCO_2 conditions, our measured pH was 0.005 ± 0.001 higher than the certified value.

Both batches of unpurified metacresol purple that had been used throughout the sampling period were tested at this occasion.

Water samples for nutrients were collected between 29 April 2015 and 7 November 2017. No pre-bloom nutrient data exist from 2015, and nutrient data were also missing for 29 August 2015 and 13 September 2016. Most nutrient samples collected in 2015 and well into May 2016 were analysed at the Institute of Marine Research, Bergen, Norway, using Alpkem Flow Solution IV or Skalar autoanalysers and employing the methods of Grasshof (1965) and Bendschneider and Robinson (1952), that is, the rapid flow analyser methodology (Alpkem 1989), for $[Si(OH)_4]$ and $[NO_3^-]$, respectively. $[NO_3^-]$ and $[Si(OH)_4]$ detection limits were 0.4 and 0.7 µmol L^{-1}, respectively. Samples from 2 May in 2015 and all samples obtained between April and August 2017 were analysed at the UiT—The Arctic University of Norway, Tromsø, using a Flow Solution IV analyser (O.I. Analytical), with methods adapted from Grasshof et al. (2009). Here, the $[NO_3^-]$ and $[Si(OH)_4]$ detection limits were 0.04 and 0.07 µmol L^{-1}, respectively. The rest of the samples were analysed at UNIS using a QuAAtro autoanalyser (SEAL Analytical, methods no. Q-068-05 Rev. 10 and no. Q-066-05 Rev. 5 for $[NO_3^-]$ and $[Si(OH)_4]$, respectively, developed by the Royal Netherlands Institute for Sea Research), with the detection limits of 0.05 and 0.04 µmol L^{-1} for $[NO_3^-]$ and $[Si(OH)_4]$, respectively. The UNIS laboratory estimated the precision (i.e., the mean absolute difference between duplicate runs) of the methods for $[NO_3^-]$ and $[Si(OH)_4]$ to be ± 0.08 and ± 0.07 µmol L^{-1}, respectively. The accuracy was on the order of ± 2–3% or better, as estimated from solutions of high-purity salts prepared for each analysis. Note that as different laboratories have analysed the nutrients samples, inter-laboratory offsets could potentially affect the data set and any interpretation thereof.

Computational methods

The marine CO_2 system. DIC, pCO_2, $[CO_3^{2-}]$, Ω_{Ar} and the Revelle factor were estimated using the CO2SYS programme (van Heuven et al. 2011), with the measured TA, pH, S, T and pressure as input parameters. The CO_2-system stoichiometric dissociation constants (K_1* and K_2*) of Mehrbach et al. (1973), as refit by Dickson and Millero (1987), were used as these have shown promising agreement between calculated and measured pCO_2 of Arctic surface waters (Chen et al. 2015; Woosley et al. 2017). Furthermore, the dissociation constant of bisulphate (K_{SO4}) of Dickson (1990) and total borate according to Lee et al. (2010) were used. K_{sp}* was estimated according to Mucci (1983) using the pressure correction of Millero (1979). $[Ca^{2+}]$ was calculated from the expression of Riley and Tongudai (1967).

The calculated marine CO_2 system properties are referred to as "observed" when presented in the following sections and have constrained uncertainties that result from uncertainties in the input parameters, as shown in the following. Firstly, values of the concentrations of phosphate and silicic acid were not included in the CO2SYS calculations, because nutrient data were missing on a few sampling occasions. This resulted in minor overestimates of the calculated properties: on average 0.5 ± 0.3 µmol kg^{-1}, 0.08 ± 0.05 µatm, 0.03 ± 0.01 µmol kg^{-1}, 0.0004 ± 0.0002 and 0.006 ± 0.004 higher values for DIC, pCO_2, $[CO_3^{2-}]$, Ω_{Ar} and the Revelle factor, respectively. Secondly, uncertainties in the calculated DIC and pCO_2 that result from uncertainties in TA, pH, S, T, K_1* and K_2* were on average ± 7 µmol kg^{-1} and ± 11 µatm, respectively, as estimated according to the DOS version of the CO2SYS software (Lewis & Wallace 1998). Finally, uncertainties in $[CO_3^{2-}]$, Ω_{Ar} and the Revelle factor were approximated to about ± 1.0–1.5 µmol kg^{-1}, ± 0.06–0.08 and ± 0.02, respectively, using a simplified Monte Carlo approach. That is, uncertainties because of the accuracy and precision/resolution in the pH, TA, S and T data were used to calculate normally distributed artificial random errors (n = 10 000) for each property with a standard deviation equal to the respective uncertainty. The errors were added to each value of each property accordingly and used as inputs in CO2SYS giving 10 000 estimates of $[CO_3^{2-}]$, Ω_{Ar} and the Revelle factor for each water sample with pH and TA data. The standard deviation of these estimates was used as the uncertainty measure for each calculated value of $[CO_3^{2-}]$, Ω_{Ar} and the Revelle factor.

Freshwater fraction. A reference salinity of 34.8 (S_{ref}), typical for TAW present at the IsA Station in winter as observed over the fieldwork period, was used to estimate the freshwater fraction (f_{fw}) according to

$$f_{fw} = \frac{(S_{ref} - S)}{S_{ref}}, \quad (2)$$

where S is the measured salinity.

Controls on the marine CO_2 system variability. Water column variability in the marine CO_2 system properties—DIC, TA and Ω_{Ar}—was investigated in terms of depth-integrated averages for each sampling occasion at the IsA Station. The sampling depths varied depending on sampling vessel and equipment, but were about 2, 10 and/or 15, 25, 50 and/or 60 m, and a maximum depth that varied between 60 and 90 m. As the sampling depths were

Citation: *Polar Research* 2019, *38*, 3345, http://dx.doi.org/10.33265/polar.v38.3345

not evenly distributed, a trapezoidal integration (assuming a linear evolution of the properties between sampling depths) was chosen to give weighted averages. The properties of relevance (T, S, p, TA, DIC and NO_3^-) were integrated from a depth of 75 m (this was chosen because it is the midpoint between 60 and 90 m) to 2 m and subsequently divided by the difference in depth (73 m). If necessary, when the sample depth was not exactly 2 or 75 m, the values at 2 and 75 m were interpolated/extrapolated from the values at the actual sampling depths for the respective sampling occasion. Note that Ω_{Ar} does not obey a linear mixing relation and is dependent on temperature and pressure. For that reason, changes in Ω_{Ar} were calculated using CO2SYS with the depth-integrated average DIC, TA, pressure, S and T as inputs.

To evaluate monthly changes, all averaged properties of relevance for each sampling occasion were used to obtain one value at the end of each month using linear interpolation. Using this time series, changes between consecutive data points were calculated and subsequently summed for each month. These monthly values are referred to as observed changes in DIC (ΔDIC_{obs}), TA (ΔTA_{obs}) and Ω_{Ar} ($\Delta\Omega_{Ar,obs}$). The changes in DIC, TA and Ω_{Ar} that result from physical and biogeochemical processes were then estimated and summed for each month.

Water column DIC is controlled predominantly by air–sea CO_2 fluxes, advection, freshwater input, mixing and biological activity (primary production and respiration), if the effects of $CaCO_3$ production/dissolution and benthic fluxes are minimal. The expected monthly changes in DIC over the upper 75 m that result from air–sea CO_2 fluxes ($\Delta DIC_{air\text{-}sea}$) were estimated according to

$$\Delta DIC_{air-sea} = \frac{\int_{t_{pm}}^{t_m} 0.251 U_{10}^2 \left(\frac{Sc}{660}\right)^{-0.5} K_0 \left(pCO_{2w} - pCO_{2a}\right) dt}{75}, \quad (3)$$

where t_m and t_{pm} refer to the timing of the end of the current and the previous month, respectively. Note that $\Delta DIC_{air\text{-}sea}$ was converted to molinity by dividing the property with the density. The flux is estimated from the gas transfer velocity expression of Wanninkhof (2014), with the squared wind speed at 10 m (U_{10}) and the Schmidt number (*Sc*) polynomial of Wanninkhof (2014), which is multiplied with the product of the solubility coefficient of CO_2 (K_0) of Weiss (1974) and the air–sea pCO_2 gradient (ΔpCO_2), that is, the difference between the partial pressure between air (pCO_{2a}) and water (pCO_{2w}). The Norwegian Meteorological Institute (eklima.met.no/) provided wind speed data at 10 m with an hourly resolution, which were measured at the weather station at Svalbard Airport (Fig. 1a). The monthly mean squared wind speed was used in the calculations. The pCO_{2a} was approximated to 400 ± 8 µatm—the average between the beginning of January 2015 and 2018—for a vapour pressure at sea level based on weather data at Svalbard Airport (obtained from the Norwegian Meteorological Institute and vapour pressure calculation according to WMO 2014), and xCO_2 data for dry air (data flagged as invalid or data with a standard deviation >1 µmol/mol were removed) from the Zeppelin Observatory, Spitsbergen (Fig. 1a; Norwegian Institute for Air Research; http://ebas.nilu.no/). pCO_{2w} was the calculated pCO_2 in the surface water and was sampled at a mean depth of 2 ± 1 m (except for 3 July 2015 when the non-linear optimization failed to estimate TA for the surface sample and the sample from 10 m was used instead).

The uncertainty (u) of the flux (F) was calculated according to Eqn. 4, including components with correlation:

$$u(F) = \left(\begin{array}{l} \left(\frac{\partial F}{\partial k} u(k)\right)^2 + \left(\frac{\partial F}{\partial K_0} u(K_0)\right)^2 \\ + \left(\frac{\partial F}{\partial \Delta pCO_2} u(\Delta pCO_2)\right)^2 \\ + 2 r_{k,K_0} \left(\frac{\partial F}{\partial k}\frac{\partial F}{\partial K_0}\right) u(k) u(K_0) \\ + 2 r_{k,\Delta pCO_2} \left(\frac{\partial F}{\partial k}\frac{\partial F}{\partial \Delta pCO_2}\right) u(k) u(\Delta pCO_2) \\ + 2 r_{K_0,\Delta pCO_2} \left(\frac{\partial F}{\partial K_0}\frac{\partial F}{\partial \Delta pCO_2}\right) u(K_0) u(\Delta pCO_2) \end{array} \right)^{1/2} \quad (4)$$

where $u(k)$ was the uncertainty in the gas transfer velocity; k value was assumed to be 20% (Wanninkhof 2014); the uncertainty in K_0, $u(K_0)$, was set to 0.2% according to Weiss (1974) and the uncertainty in ΔpCO_2, $u(\Delta pCO_2)$, ranged betwe 5 and 29% (using the standard deviation in pCO_{2a} of ± 8 µatm and the mean uncertainty in pCO_{2w} of ± 11 µatm found above, the relative uncertainty in ΔpCO_2 was calculated as $(8^2+11^2)^{1/2}|\Delta pCO_2|^{-1}$). The time series of the calculated k, K_0 and ΔpCO_2 was used to calculate the correlation coefficient (r) of each combination (k and K_0, k and ΔpCO_2, and K_0 and ΔpCO_2), resulting in r_{k,K_0}, $r_{k,\Delta pCO_2}$ and $r_{K_0,\Delta pCO_2}$ of 0.09, 0.51 and 0.16, respectively.

Without the influence of the air–sea CO_2 flux and also biology, DIC would mix conservatively. The changes in DIC that result from the combined effects of river runoff, mixing of different water masses, advection and, to a lesser extent, precipitation and evaporation ($\Delta DIC_{adv/rro}$)

were therefore estimated from changes in salinity according to the DIC-S relationship below

$$DIC = 52.1S + 339, \quad (5)$$

which is based on a mixing line made between land runoff (DIC = 339 µmol kg^{-1}, S = 0; Ericson et al. 2018) and wintertime TAW (DIC = 2152 µmol kg^{-1}, S = 34.8 as estimated from mean January to March data). This mixing line lies very close to the corresponding mixing line between ArW (i.e., DIC = 2138 µmol kg^{-1}, S = 34.6, also estimated for mean January to March data) and land runoff; the slopes differ with 0.2 %. For this reason, the two water masses are treated as one, and changes in salinity and DIC because of the presence of TAW, ArW and/or land runoff mixed with either of the former two are expected to follow the mixing line in Eqn. 5 as well.

The changes in DIC that result from changes in the balance between primary production and respiration (ΔDIC_{bio}) were calculated from the following expression:

$$\Delta DIC_{bio} = \left(\Delta DIC_{obs} - \Delta DIC_{air-sea} - \Delta DIC_{adv/rro}\right) \quad (6)$$

Note that the biological term will include potential effects of $CaCO_3$ production/dissolution and benthic fluxes, of which the former would result in changes twice as large for TA as for DIC.

Changes in TA were assumed to be mainly driven by river runoff, mixing of different water masses and advection of different water masses ($\Delta TA_{adv/rro}$). Measured TA versus salinity is shown in Fig. 2a. $\Delta TA_{adv/rro}$ was estimated from changes in salinity according to the relationship between changes in the depth-integrated average TA (ΔTA) and S (ΔS) shown in Fig. 2b and expressed as:

$$\Delta TA = 48.7\Delta S + 0.2 \quad (7)$$

The intercept of 0.2 of the relationship is close to zero, which indicates that other processes affecting TA—biological activity, benthic fluxes and $CaCO_3$ production/dissolution—are minimal. Still, a residual term (ΔTA_{res}) was also calculated, that is, the difference between ΔTA_{obs} and $\Delta TA_{adv/rro}$, which represents the combined effects of the above-mentioned but neglected processes and the measurement uncertainty of ± 3.3 µmol kg^{-1}.

Changes in Ω_{Ar} were investigated in terms of temperature effects, advection, mixing and river runoff, biological activity, air–sea CO_2 fluxes and changes in TA that are not related to changes in salinity. The thermodynamic dependency of Ω_{Ar} on temperature was investigated using CO2SYS with the depth-integrated average TA, DIC and

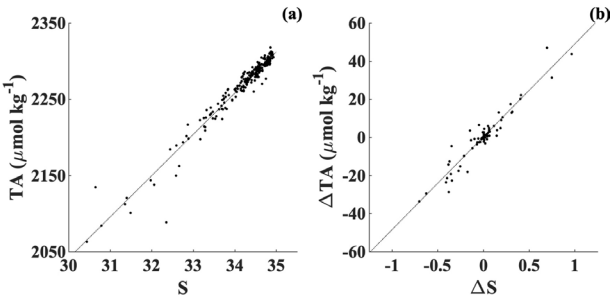

Fig. 2. (a) TA versus S with the fitted line: TA = 54.1S + 418 µmol kg^{-1} (n = 244, r^2 = 0.95). Standard errors of the slope and intercept are ±0.8 (p << 0.01) and ±27 µmol kg^{-1} (p << 0.01), respectively, and (b) changes in the depth-integrated average TA (ΔTA) versus changes in the depth-integrated average S (ΔS) with the linear fit: $\Delta TA = 48.7\Delta S + 0.2$ µmol kg^{-1} (n = 43, r^2 = 0.92), and the standard errors of the slope and intercept of ± 2.3 (p << 0.01) and ±0.9 µmol kg^{-1} (p = 0.8), respectively.

S of the previous sampling occasion as inputs, together with the depth-integrated average T of the current and the previous sampling occasions, to calculate a perturbed and an unperturbed Ω_{Ar}, respectively. The difference between the perturbed and unperturbed values gives the corresponding change in Ω_{Ar} caused by the change in temperature.

A seasonal difference in salinity of about 4 was observed at the IsA Station by Ericson et al. (2018). The correspondent change in Ω_{Ar} because of the purely thermodynamic relationship between Ω_{Ar} and salinity is very small. The salinity effect was for that reason combined with the effects of salinity-related changes in TA and DIC on Ω_{Ar}. $\Delta DIC_{adv/rro}$, $\Delta TA_{adv/rro}$ and ΔS were added to the depth-integrated average DIC, TA and S, respectively, of the previous sampling occasion. These were used as inputs in CO2SYS together with the depth-integrated average T of the previous sampling occasion to calculate a perturbed Ω_{Ar}. The change in Ω_{Ar} caused by the combined effects of river runoff, mixing and advection was estimated from the difference between the perturbed value and the unperturbed Ω_{Ar}.

The effect of biological processes on Ω_{Ar} was estimated using ΔDIC_{bio}. This property was added to the depth-integrated average DIC of the previous sampling occasion, and CO2SYS was used to calculate a perturbed Ω_{Ar} at the input conditions of the previous sampling occasion. Note that the impact of biological processes on TA is considered minimal, which is supported by Eqn. 7, and therefore neglected. The change in Ω_{Ar} because of biological processes was estimated from the difference between the perturbed value and the unperturbed Ω_{Ar}. The change in Ω_{Ar} that results from the air–sea CO_2 flux was estimated using $\Delta DIC_{air-sea}$, with the same method as described for

Citation: *Polar Research* 2019, *38*, 3345, http://dx.doi.org/10.33265/polar.v38.3345

the estimate of the change in Ω_{Ar} because of biological processes.

Finally, the change in Ω_{Ar} that is explained by the variability in TA (biological activity, $CaCO_3$ production/dissolution and measurement uncertainty), which is unrelated to changes in salinity, was estimated by adding the residual change in TA to the depth-integrated average TA of the previous sampling occasion. This value together with the other properties at the previous sampling occasion was used as input in CO2SYS, and the difference between the perturbed Ω_{Ar} and the unperturbed Ω_{Ar} was again calculated. A residual change in Ω_{Ar} was also calculated; this is the difference between the observed change in Ω_{Ar} and the sum of the calculated process driven changes.

Net community production. NCP was estimated from ΔDIC_{bio} and the change in the depth-integrated average $[NO_3^-]$, which was normalized to the mean depth-integrated average salinity of 34.3 ($\Delta[NO_3^-]_{S=34.3}$) to remove effects of salinity changes on $[NO_3^-]$. As $[NO_3^-]$ can be depleted while both DIC and $[Si(OH)_4]$ continue to be consumed, as observed in 2017, other nitrogen sources, such as ammonium, for example, could be important at the site. This excess carbon uptake could also be explained by the production of N-poor organic material (Kähler & Koeve 2001). Regardless of the cause of this carbon fixation, to capture it, ΔDIC_{bio} and $\Delta[NO_3^-]_{S=34.3}$ were first summed over the period when $[Si(OH)_4]$ and DIC drop from winter values (sometime between April and May) to the yearly minimum in $[Si(OH)_4]$ sometime in June. This period agrees with the period when ΔDIC_{bio} typically is negative (i.e., primary production exceeds respiration). The summed changes were subsequently integrated over the water column

$$NCP_{DIC} = \int_{2}^{75} -\Delta DIC_{bio}\, dz \quad (8a)$$

$$NCP_{NO_3} = \int_{2}^{75} -\Delta[NO_3^-]_{S=34.3} R_{C:N}\, dz \quad (8b)$$

$R_{C:N}$ is the Redfield stoichiometric ratio (Redfield et al. 1963), which was chosen according to the observed seston C:N ratios of 6.7 and 7.9 for AW and ArW in the Barents Sea, respectively (Frigstad et al. 2014). For the year 2016, where there are measurements for the whole year, the calculations were also done for the entire year and not only for the productive season.

Note that the productive season at the IsA Station typically is short, lasting from April to June, which could be a result of unfavourable light conditions because of sediment load in the freshwater dcharge in summer. For instance, Marquardt et al. (2016) observed very little photosynthetically active radiation (0.3 µmol m^{-2} s^{-1} at a depth of 25 m) at the station in July 2012, which coincided with a fluorescence of only 0.05. Similar conditions have been observed in other glacial-influenced Svalbard fjords such as in Kongsfjorden (Lydersen et al. 2014) and were observed in the Isfjorden system (Tempelfrden) repeatedly in August/September (visual observation, A. Fransson).

The C:N ratio was investigated for the month of major productivity in 2016 and 2017 by calculating the ratio between the monthly changes in ΔDIC_{bio} and $\Delta[NO_3^-]_{S=34.3}$ referred to hereafter as ΔC:ΔN. For the year 2016, the calculations were also done for all the other months.

Uncertainty assessment. Uncertainties in the calculated effects of the physical and biogeochemical processes on DIC, TA and Ω_{Ar}, the NCP estimates, the ΔC:ΔN ratios and the integrated net annual air–sea CO_2 flux were estimated as follows.

Uncertainties in the marine CO_2 system properties and the air–sea CO_2 flux, both discussed earlier in this article, as well as S, T, the DIC–S relationship in Eqn. 5, the TA–S relationship in Eqn. 7, $[NO_3^-]$ and $R_{C:N}$ were used to calculate artificial normally distributed random errors (n = 10 000 for each property) with a standard deviation equal to the respective uncertainty. Uncertainties in S and T are based on the combined uncertainty associated with the accuracy and resolution of the SAIV A/S SD204 CTD: ± 0.02 and ± 0.01°C for S and T, respectively. The uncertainty in the DIC:S ratio was set to ± 5 µmol kg^{-1}, to reflect the standard error of the linear regression slope for measured salinity versus calculated DIC for S < 34 (not shown); these are typical conditions over the melt season when $[NO_3^-]$ is close to depletion in the upper 15–25 m (minimum new production that affects DIC). The uncertainties in Eqn. 7 are based on the standard errors of the regression line in Fig. 2b. The uncertainty in $[NO_3^-]$ was set to ± 7%, that is, the relative standard deviation in $[NO_3^-]$ during March 2016, when the variability was large and particularly high values were observed on 4 and 29 March. The uncertainty in $R_{C:N}$ was set to ± 1 to reflect the various estimates of the Redfield elemental stoichiometric ratio that exist in the literature (e.g., 6.6, Redfield et al. 1963; 8.3, Sterner et al. 2008; Arctic Ocean mean value of 7.9, Frigstad et al. 2014).

The random errors of each property were added to each value of the respective property; there were 10 000 versions of each value. The effects of the different processes on DIC, TA and Ω_{Ar}, the NCP estimates, the ΔC:ΔN ratios and the integrated net annual air–sea CO_2 flux were calculated for 10 000 iterations. The standard

deviations of the results from the 10 000 iterations were used as uncertainty estimates. Note that these uncertainties do not account for uncertainties in the assumptions that form the basis for Eqns. 3–8.

Results

Seasonal variability

The temporal evolution of water column temperature, salinity, f_{fw}, TA, DIC, pH, pCO_2, $[CO_3^{2-}]$, Ω_{Ar}, the Revelle factor, $[NO_3^-]$ and $[Si(OH)_4]$ are shown in Fig. 3 (between 2 and 75 m). Temperature (Fig. 3a) fluctuated between summer peaks of about 6°C to 9°C in the surface which coincided with minima in salinity of less than 31 (Fig. 3b) and winter lows in March and April of −1.5°C to 1°C. Winter temperature and salinity were more homogeneous with depth compared to the conditions in summer. Late winter (March–April) salinity was less than 34.6 in 2015 (i.e., ArW), which coincided with the coldest water column (<0°C). The corresponding salinity the following winters was higher than 34.7 with a temperature of about 1°C or more (i.e., TAW), although in 2017 there was a shift from higher salinities (>34.7) to lower salinities (<34.6), which took place sometime between 3 April and 4 May. The effect of meltwater runoff was apparent in the salinity and f_{fw} (Fig. 3c) time series, where the freshwater contribution reached a maximum of 10–11% in August. This seasonal pattern was also reflected in the temporal variability of TA (Fig. 3d) and DIC (Fig. 3e). TA ranged between ca. 2060 and 2310 µmol kg^{-1}, with the lowest concentrations in the summer months and early

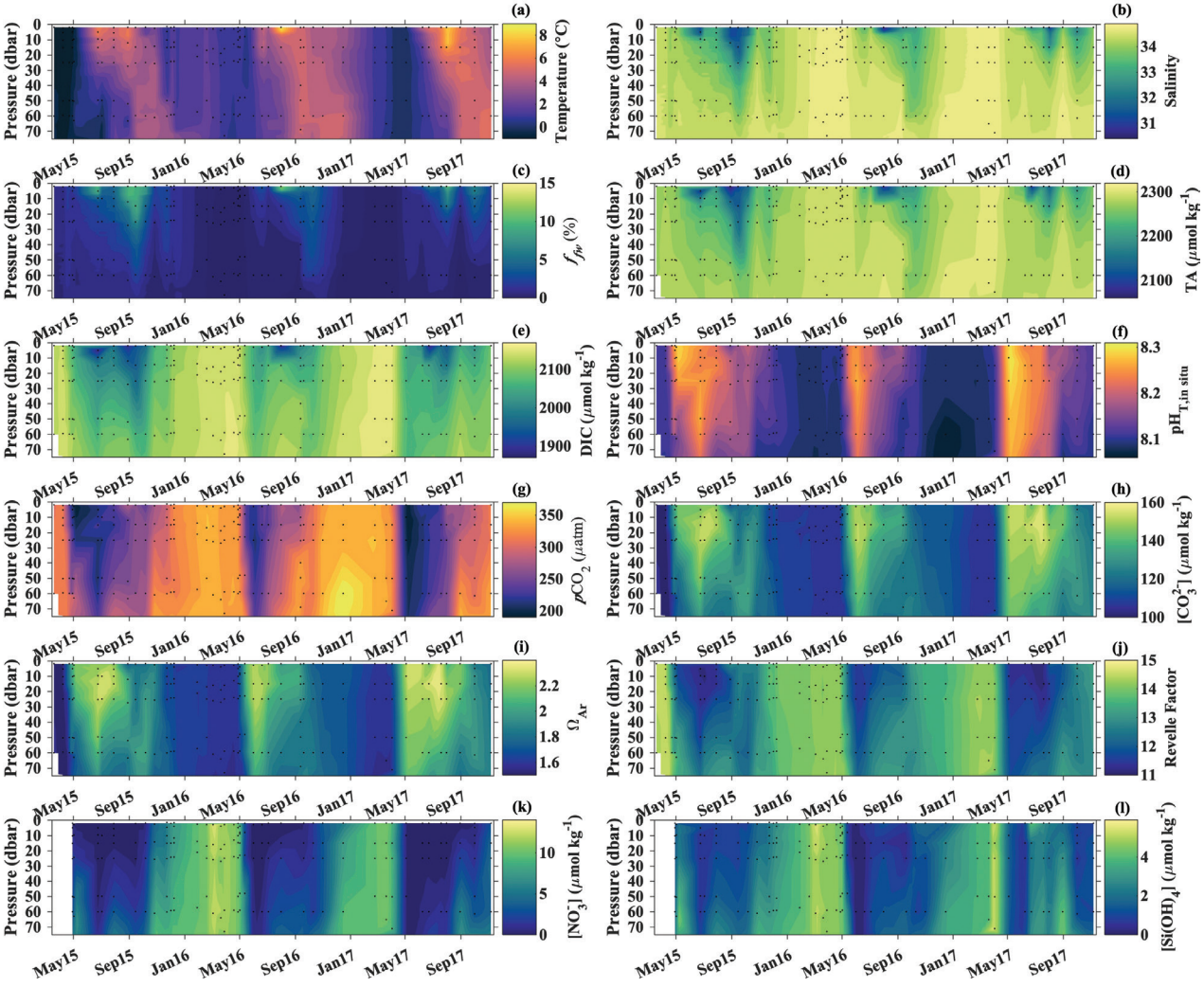

Fig. 3. Time series of water column properties (2–75 m): (a) temperature, (b) salinity, (c) f_{fw} (freshwater fraction), (d) TA, (e) DIC, (f) pH, (g) pCO_2, (h) $[CO_3^{2-}]$, (i) Ω_{Ar}, (j) the Revelle factor, (k) $[NO_3^-]$ and (l) $[Si(OH)_4]$ at the IsA Station. Black dots show the timing of sampling as well as the sampling depths.

Citation: *Polar Research* 2019, *38*, 3345, http://dx.doi.org/10.33265/polar.v38.3345

autumn (June–September) and the highest values in winter and early spring (January to April). DIC followed a similar pattern as TA, but low DIC concentrations of roughly 2050 to 2060 µmol kg^{-1} were already observed between April and June. This coincided with low [NO_3^-] (<0.4 µmol kg^{-1}; Fig. 3k) and low [$Si(OH)_4$] (minima in June of < 0.7 µmol kg^{-1}; Fig. 3l), reflecting biological CO_2 consumption. DIC decreased even further by input of freshwater during the summer season from June to August, with minima in the surface water <1900 µmol kg^{-1}. Winter DIC ranged from 2130 to 2170 µmol kg^{-1}, with values in the higher range when the salinity was higher (S > 34.7). [NO_3^-] remained low (<0.4 µmol kg^{-1}) in the upper water column throughout the summer season, whereas [$Si(OH)_4$] was more variable, with concentrations that ranged from <0.7 to 4.6 µmol kg^{-1}. Typical winter values for [NO_3^-] and [$Si(OH)_4$] were about 10–11 and 4–5 µmol kg^{-1}, respectively, except for on 4 and 29 March 2016, when [NO_3^-] and [$Si(OH)_4$] were especially high, ranging between 11.4–13.8 and 4.7–5.9 µmol kg^{-1}.

The biological CO_2 drawdown was also reflected in in situ pH (Fig. 3f) and pCO_2 (Fig. 3g), and coincided with yearly maxima in pH of about 8.30 and minima in pCO_2 of roughly 190–210 µatm sometime between April and June depending on year. The minimum of pCO_2 was slightly higher in 2016 compared to the other two years. Water column pCO_2 was less than the atmospheric pCO_2 throughout the study period and the air–sea pCO_2 gradient was thereby negative. This allows for atmospheric CO_2 uptake by the surface water. pH decreased with depth and reached a minima of about 8.07–8.09 during the winters of 2015/16 and 2016/17, when the water temperature was higher (between 1 and 4°C) than that in 2015. These minima in pH also coincided with the maxima in pCO_2 of 340–370 µatm.

Both pH and pCO_2 are sensitive to temperature and salinity changes. An increase in temperature of roughly 7°C in the surface water over the winter to summer season results in a pH decrease of ca. 0.11 units ($dpH/dT \approx -0.016°C^{-1}$; Millero 2007) and pCO_2 increase of ca. 30% ($dlnpCO_2/dT \approx 0.0423°C^{-1}$; Takahashi et al. 1993). In contrast, the decrease in salinity of about 4 in the surface water over the summer season increases the pH by ca. 0.06 units and decreases the pCO_2 by roughly 20% (ca. 10% due to the thermodynamic dependence of pCO_2 on salinity and ca. 10% because of the dilution of DIC and TA, as estimated using CO2SYS for the S range: 30.4–34.9, and the correspondent DIC and TA according to Eqn. 5 and the linear fit in Fig. 2a, respectively).

Similar to pH, the biological uptake of DIC resulted in increased [CO_3^{2-}] (Fig. 3h) and hence Ω_{Ar} (Fig. 3i) to about 140–150 µmol kg^{-1} and 2.2–2.3, respectively, in the upper parts of the water column. These properties remained high during the summer with occasional maxima in 2015 and 2017 of up to 150–160 µmol kg^{-1} and 2.3–2.4 for [CO_3^{2-}] and Ω_{Ar}, respectively. The high values both in spring and summer coincide with the largest TA:DIC ratio observed of about 1.11 and the highest CO_2 buffer capacity with the Revelle factor (Fig. 3j) of ca. 11–12. The minima in [CO_3^{2-}] and Ω_{Ar} of 101 µmol kg^{-1} and 1.5, respectively, was observed at the onset of the study, when cold and less saline water (T < 0°C and S < 34.7) dominated the water column. This also coincided with the lowest observed TA:DIC ratio of ca. 1.06 and the lowest CO_2 buffer capacity, that is, a maximum in the Revelle factor of about 14.7. The Revelle factor was about 14 the following winters, when the salinity was higher than 34.7 and [CO_3^{2-}] was ca. 110 µmol kg^{-1} and Ω_{Ar} was 1.6.

Drivers of the marine CO_2 system

Physical and biogeochemical controls on DIC, TA and Ω_{Ar} are presented in Fig. 4, for each month studied in the years 2015, 2016 and 2017. The relative contributions of the individual processes as observed over the entire study period are presented in Table 1. The variability in DIC was mainly governed by biological processes (relative impact of 44± 1%) and advection/mixing/river runoff (relative impact of 45 ± 1%), of which the former resulted in monthly changes that ranged from −70 to 20 µmol kg^{-1}. The major CO_2 drawdown took place in April in 2015 (Fig. 4a) and 2017 (Fig. 4g). For these two years, the spring bloom signature in terms of low pCO_2 (ca. 190–220 µatm), low DIC (<2100 µmol kg^{-1}) and low [NO_3^-] (<<10 µmol kg^{-1}) coincided with water

Table 1 Relative impact in per cent of different processes on DIC, TA and Ω_{Ar}.

Property	Air–sea[a]	adv/rro[b]	bio[c]	T[d]	TA residual	Ω_{Ar} residual
ΔDIC	11 ± 0.3	45 ± 1	44 ± 1	–	–	–
ΔTA	–	77 ± 1	–	–	23 ± 1	–
$\Delta\Omega_{Ar}$	15 ± 0.5	5 ± 1	60 ± 2	3 ± 0.1	18 ± 1	0.4 ± 0.04

[a]CO_2 gas exchange. [b]Advection, river runoff and mixing. [c]Biological processes. [d]Temperature. The uncertainties were calculated as outlined in the subsection on uncertainty assessment, in the section on computational methods.

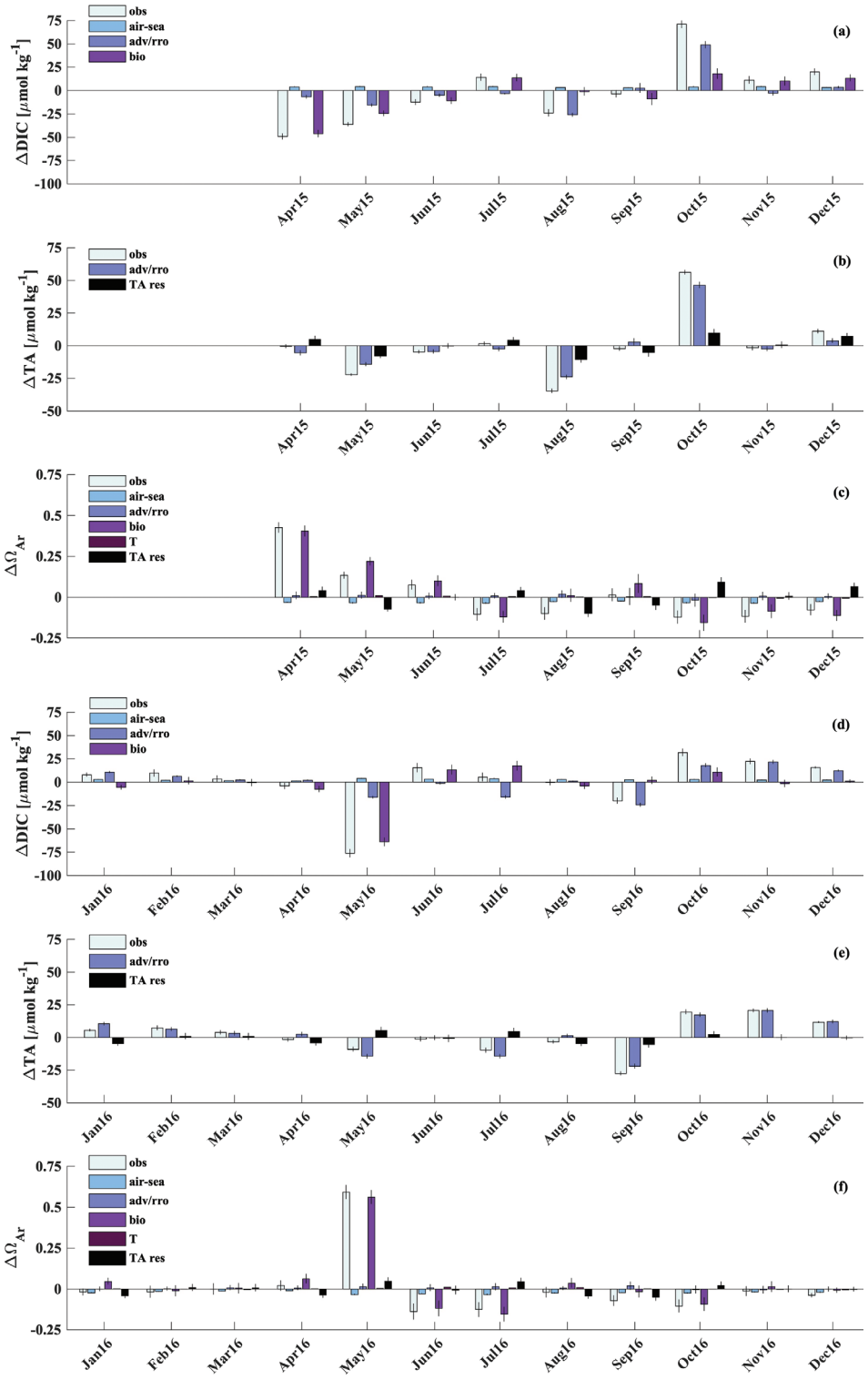

Fig. 4. Controls on: (a) DIC, (b) TA and (c) Ω_{Ar} in 2015; (d) DIC, (e) TA and (f) Ω_{Ar} in 2016; and (g) DIC, (h) TA and (i) Ω_{Ar} in 2017. Changes (obs = observed, air–sea = CO_2 gas exchange, adv/rro = advection, river runoff and mixing, bio = biological processes, T = temperature, TA res = TA residual) are expressed for depth-integrated averages where the water column extends from 2 to 75 m. Also note that no data were collected in January and September 2017, and changes for these months are based on interpolated values. The uncertainties were calculated as outlined in the subsection on uncertainty assessment, in the section on computational methods. (Figure is continued on next page.)

Citation: *Polar Research* 2019, *38*, 3345, http://dx.doi.org/10.33265/polar.v38.3345

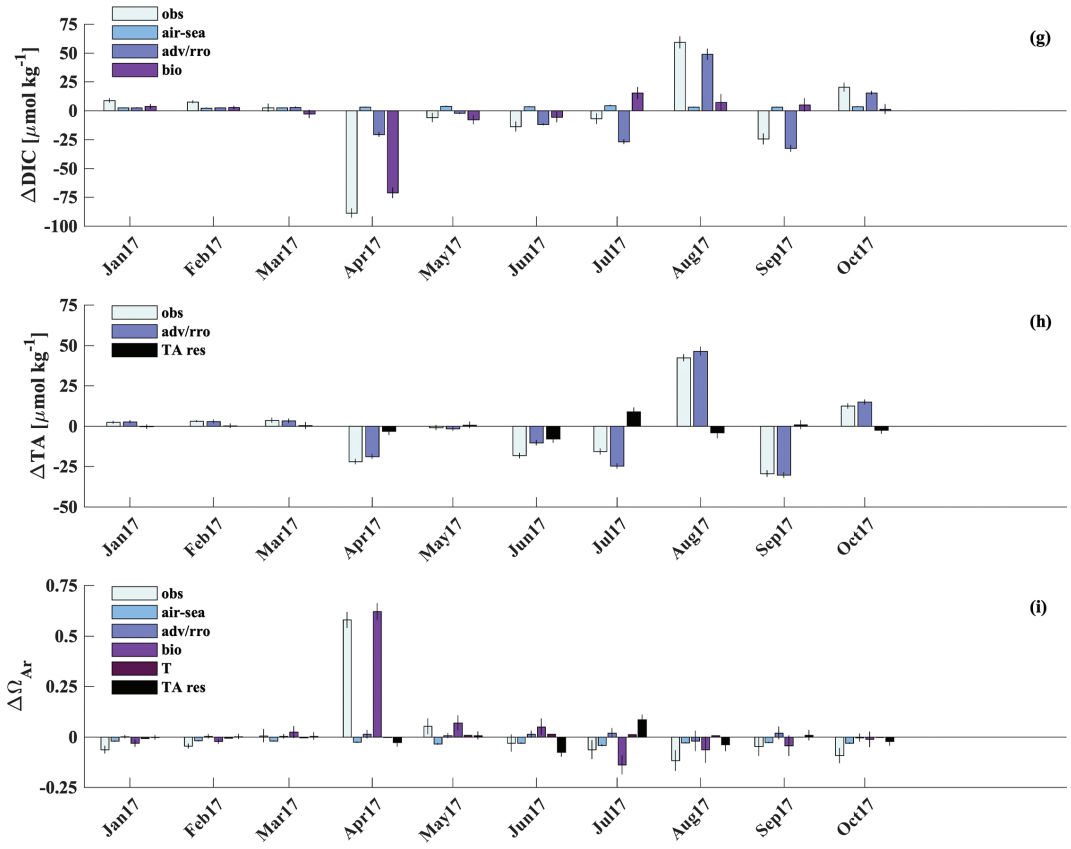

Fig. 4. (Continued from previous page.) Controls on: (a) DIC, (b) TA and (c) Ω_{Ar} in 2015; (d) DIC, (e) TA and (f) Ω_{Ar} in 2016; and (g) DIC, (h) TA and (i) Ω_{Ar} in 2017. Changes (obs = observed, air–sea = CO_2 gas exchange, adv/rro = advection, river runoff and mixing, bio = biological processes, T = temperature, TA res = TA residual) are expressed for depth-integrated averages where the water column extends from 2 to 75 m. Also note that no data were collected in January and September 2017, and changes for these months are based on interpolated values. The uncertainties were calculated as outlined in the subsection on uncertainty assessment, in the section on computational methods.

column salinities <34.7 (Fig. 3b) and temperatures <0.2°C (Fig. 3a). In 2016 when the winter temperature was about 1°C (Fig. 3a) and the salinity was larger than 34.7 (Fig. 3b), the bloom began in May, a couple of weeks later compared to the other two years (Fig. 4d). The biological fixation of DIC into organic matter during the productive season resulted in a drop in DIC of ca. 70 to 90 µmol kg^{-1}, with the largest change in 2015. The productive season was altogether fairly short, lasting for 1–3 months and typically ending when the melt season took off in June, which coincided with low nutrient concentrations in the upper water column (Fig. 3k, l). Roughly half of the net biological CO_2 consumption was balanced by a net heterotrophic water column for most of the remaining year. The other half was compensated for by air–sea CO_2 uptake (relative impact of 11 ± 0.3%) that resulted in modest monthly changes between 1 and 5 µmol kg^{-1}.

Between May and August, the freshening of the surface layer resulted in monthly decreases in DIC and TA of up to 30 µmol kg^{-1} (Fig. 4a, b, d, e, g, h). Advection of, or mixing with, more saline waters during late summer and autumn resulted in monthly increases of DIC and TA, with the maximum change being close to 50 µmol kg^{-1}. The variability during winter, between January and March, was typically in the order of the uncertainty in the measured TA and the calculated DIC. The residual change in TA was on average −0.3 µmol kg^{-1} with a standard deviation of 4.9 µmol kg^{-1}, which is not much different from the measurement uncertainty (± 3.3 µmol kg^{-1}). Still this variability had a relative contribution of 23 ± 1% as compared to the 77 ± 1% that was accounted for by advection/mixing/river runoff (Table 1).

The variability in Ω_{Ar} was essentially explained by biological processes (relative impact of 60 ± 2%; Table 1 and Fig. 4c, f, i) that resulted in shifts in the TA:DIC

ratio. Biological CO_2 consumption resulted in monthly increases in Ω_{Ar} of up to 0.62. When the system was net heterotrophic, respiration (CO_2 production) resulted in decreases in Ω_{Ar} of about 0.16 or less. The air–sea CO_2 uptake was responsible for monthly decreases in Ω_{Ar} of 0.03 on average with a standard deviation of 0.01, which when added together resulted in a relative impact of 15 ± 0.5% of the overall Ω_{Ar} variability. The residual changes in TA were on average responsible for monthly changes in Ω_{Ar} of −0.003 with a standard deviation of 0.045. The other processes were of minor importance. Advection/mixing/river runoff resulted in mean monthly changes in Ω_{Ar} of 0.005 with a standard deviation of 0.010, and temperature resulted in mean monthly changes in Ω_{Ar} of 0.002 with a standard deviation of 0.006. The residual change in TA was responsible for 18 ± 1% of the Ω_{Ar} variability, whereas advection/mixing/river runoff and temperature contributed with 5 ± 1% and 3 ± 0.1%, respectively (Table 1).

Net community production

NCP_{DIC} and NCP_{NO_3} during the three productive seasons between 2015 and 2017 are presented in Table 2. Note that NCP_{NO_3} only was estimated for the latter two years, for which nutrient data exist at the onset of the phytoplankton bloom. NCP_{DIC} ranged between 65 and 85 g C m^{-2}, with the lowest value coinciding with the presence of TAW in 2016. ArW dominated the water column during the spring of 2015, and it was also the water mass that coincided with low nutrient concentrations, DIC and pCO_2 values that are typical for bloom periods as observed in the beginning of May in 2017. Figure 5 shows the timing of TAW/AW presence at the IsA Station, but note that the timing is sensitive to the interpolation of the actual measurements. The seasonal NCP_{NO_3} was 67 ± 10 g C m^{-2} in 2016, as estimated for a $R_{C:N}$ of 6.7 typical for AW in the nearby Barents Sea (Frigstad et al. 2014), and 66 ± 10 g C m^{-2} in 2017 for a $R_{C:N}$ of 7.9, as observed for ArW in the Barents Sea (Frigstad et al. 2014).

Over the full annual cycle in 2016, the integrated NCP_{DIC} was 34 ± 6 g C m^{-2} yr^{-1}, which can be compared to the corresponding value for NCP_{NO_3} of 2 ± 1 g C m^{-2} yr^{-1}. This discrepancy between NCP_{DIC} and NCP_{NO_3} will be discussed below. The impact of the net uptake of carbon by phytoplankton on the water column DIC was counteracted by the integrated annual air–sea CO_2 flux (oceanic uptake of carbon) of about −29 ± 2 g C m^{-2} yr^{-1}, as estimated for the same year.

Table 2 Seasonal and annual net community production (NCP) (in g C m^{-2} and g C m^{-2} yr^{-1}, respectively) as estimated from ΔDIC_{bio} and $\Delta[NO_3^-]_{S=34.3}$, the annual air–sea CO_2 flux (F_{CO_2}, g C m^{-2} yr^{-1}) and the ΔC:ΔN ratio at the IsA Station for the month of major productivity. The uncertainties were calculated as outlined in the subsection on uncertainty assessment, in the section on computational methods.

Year	Seasonal			Annual			Month	ΔC:ΔN
	NCP_{DIC}	NCP_{NO_3}	NCP_{NO_3}	NCP_{DIC}	NCP_{NO_3}	F_{CO_2}		
2015	84.5 ± 4.8	–	–	–	–	–	–	–
2016	64.9 ± 5.0	67.1 ± 10.0[a]	66.2 ± 10.0	34.2 ± 5.6	2.5 ± 0.7[a]	−29.4 ± 1.5	May	6.6 ± 0.5
2017	72.6 ± 4.8	66.1 ± 8.4[b]	72.8 ± 8.3	–	–	–	April	8.7 ± 0.6

[a]$R_{C:N}$ of Frigstad et al. (2014) for AW: $R_{C:N}$ = 6.7. [b] $R_{C:N}$ of Frigstad et al. (2014) for ArW: $R_{C:N}$ = 7.9.

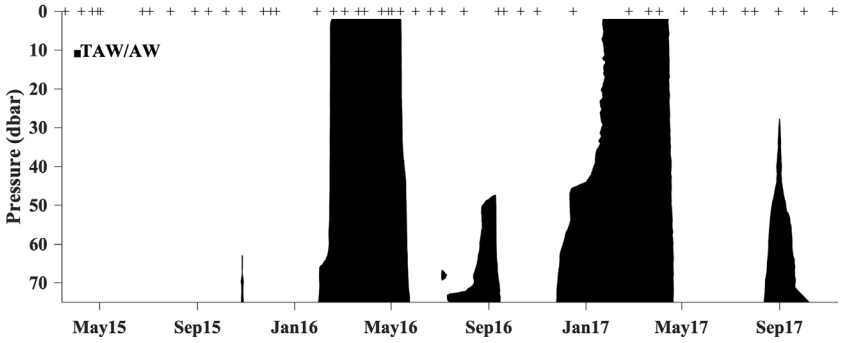

Fig. 5. Filled contour plot showing the presence of TAW/AW (S ≥ 34.7) in black with crosses showing the actual sampling occasions.

Citation: *Polar Research* 2019, *38*, 3345, http://dx.doi.org/10.33265/polar.v38.3345

Discussion

Drivers of the marine CO_2 system

The variability in DIC and Ω_{Ar} (Eqn. 1) was largely governed by biological processes, with relative contributions of 44% for DIC and 60 ± 2% for Ω_{Ar} (or, if excluding the effect of the residual variation in TA, 73%). Fransson et al. (2016) presented a similar conclusion for the glacier-influenced waters of Kongsfjorden (west Spitsbergen) further north, where the biological activity was suggested to account for 46–55% of the variability in Ω_{Ar}. That biological processes are one of the major drivers of Ω_{Ar} have also been found in other parts of the Arctic Ocean, for example, in the Amundsen Gulf in the south-eastern Beaufort Sea, where biological processes contributed 52% of the total variability in Ω_{Ar} (Chierici et al. 2011). While the relative contributions to some extent agree, this reflects the choice of investigated processes for the specific study sites as well as the underlying methods to determine the effects. In the Amundsen Gulf, biological activity accounted for monthly changes in Ω_{Ar} of −0.23 to 0.17 month^{-1} (taken from figure 7 in Chierici et al. 2011), whereas the changes in Ω_{Ar} at the IsA Station were considerably larger: −0.16 to 0.62 month^{-1}. The discrepancy between the two is difficult to assess because of differences in the methodology, but could reflect lower nitrate availability (about 5 µmol L^{-1} according to figure 5e in Chierici et al. 2011) in the surface layer of the Amundsen Gulf at the start of the biological production as compared to the IsA Station (10–11 µmol kg^{-1}). For the entire productive period, the CO_2 consumption at the IsA Station resulted in increases in Ω_{Ar} of 0.6–0.7, which can be compared to increases in Ω_{Ar} of 0.6–0.9 in Kongsfjorden (Fransson et al. 2016). The corresponding value in the Amundsen Gulf was about 0.3, which is half or less than that in the western Spitsbergen fjords.

Freshwater runoff, mixing and advection resulted in a seasonal variability in salinity of about 4 and contributed with 77 ± 1% and 45 ± 1% of the monthly changes in TA and DIC, respectively. The corresponding contribution to the Ω_{Ar} variability, on the other hand, was only 5 ± 1%, and the monthly changes in Ω_{Ar} were in the order of −0.02 to 0.02 month^{-1}. The reason for this is that these processes affect both DIC and TA, which results in minimal changes in the TA:DIC ratio. Also, the seasonal warming and cooling resulted in minor changes in Ω_{Ar} of −0.01 to 0.01 month^{-1}, with an overall relative impact of 3 ± 0.1%. In this regard, the waters of Adventfjorden may not be very sensitive to further warming because of climate change, with subsequent glacial and snow melt discharges. This is in contrast to the study by Fransson et al. (2016) in Kongsfjorden further north, where future increased warming was suggested to have significant impact on glacial meltwater and consequently Ω_{Ar}. The authors estimated that a freshwater fraction of 10–11% results in a reduction in Ω_{Ar} of 0.7 based on dilution scenarios for different end-member TA. The corresponding freshwater fraction of 10% at the IsA Station reduces Ω_{Ar} by only 0.09 (for DIC according to Eqn. 5 and TA according to the linear fit in Fig. 2a).

Even though the freshwater inflow at the IsA Station reduces Ω_{Ar} by only 0.009/% f_{fw} over a period when Ω_{Ar} typically is at its yearly maximum, the Ω_{Ar} of the winter ArW is 1.5. Similar values have been observed in Kongsfjorden (Ω_{Ar} ca. 1.5 in the deep water; Fransson et al. 2016) and in Tempelfjorden, a neighbouring branch within the Isfjorden system (Ω_{Ar} ca. 1.3–1.6 in the surface water; Fransson et al. 2015). With this in mind, and adding that increased meltwater releases are likely to bring more riverine organic decay products that contribute to increased CO_2, it seems reasonable to assume that Ω_{Ar} at least may be sensitive to future increases in freshwater discharges.

Net community production

The importance of biological processes on the marine CO_2 system, through the consumption or production of CO_2, is also reflected in the seasonal NCP drawdown that ranged from 65 to 85 g C m^{-2}. This is higher than a DIC-based seasonal NCP drawdown for the Amundsen Gulf region of 49 g C m^{-2} (productive season from April to August, Shadwick et al. 2011). The range is also higher than nutrient-based seasonal NCP estimates for the Nordic and Barents seas as well as for the Canadian Arctic Archipelago of 30–40 g C m^{-2} (Codispoti et al. 2013).

The annually integrated NCP_{DIC} of 34 ± 1 g C m^{-2} yr^{-1} was considerably larger than the corresponding NCP_{NO_3} of 2 ± 1 g C m^{-2} yr^{-1}. This discrepancy could reflect the sensitivity of nutrient-based NCP estimates to the choice of the Redfield stoichiometric regeneration ratio that cannot constrain carbon overconsumption that may occur when nitrate becomes depleted. The use of the C:N Redfield ratio for the whole year will therefore result in a too low NCP_{NO_3}. To illustrate this, monthly ΔC:ΔN ratios at the IsA Station were estimated for the annual cycle of 2016, as shown in Fig. 6.

Note that the monthly changes in $\Delta[NO_3^-]_{S=34.3}$ were minimal (<0.05 µmol kg^{-1}) in August and September 2016 giving unreasonably high ΔC:ΔN values, and these ratios are therefore not shown. The annual cycle in the ΔC:ΔN ratio at the IsA Station shows high values (>10) in the summer (June–July), which likely reflect carbon

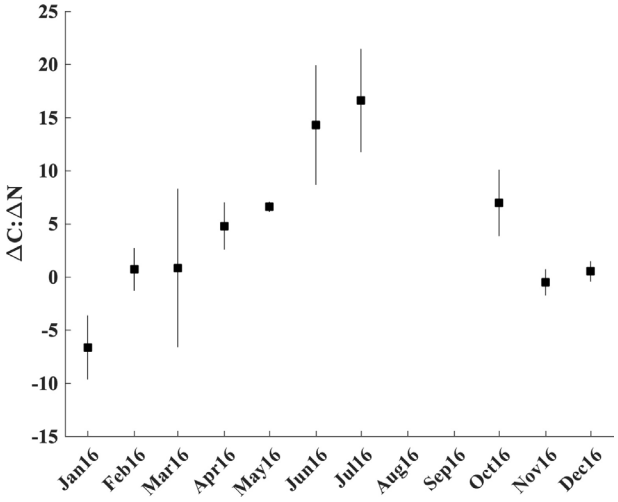

Fig. 6. ΔC:ΔN ratios for the IsA Station as estimated from monthly changes in ΔDIC_{bio} and $\Delta[NO_3^-]_{S=34.3}$. Ratios for August and September for which $\Delta[NO_3^-]_{S=34.3} < 0.05$ µmol kg^{-1} are not included as they are unrealistically high on account of depleted nitrate values. The uncertainties were calculated as outlined in the subsection on uncertainty assessment, in the section on computational methods.

overconsumption as observed in the north-east Atlantic (Kähler & Koeve 2001), and low values (<1) in the winter season (November–March), when the magnitude of the changes in DIC caused by biological processes was small (<6 µmol kg^{-1}). The values should be interpreted with care as they depend on the scaling of the gas transfer velocity of the air–sea CO_2 exchange (Eqn. 3) as well as on the DIC–S relationship in Eqn. 5. While the uncertainty in the ΔC:ΔN ratio during the month of major productivity is fairly well constrained (<1), the uncertainty during the other months is 2–15 times larger. The negative ratio in January reflects the negative ΔDIC_{bio} of −5 µmol kg^{-1} (Fig. 4e), that is, ΔDIC_{obs} (ca. 8 µmol kg^{-1}) was smaller than the sum of $\Delta DIC_{air\text{-}sea}$ and $\Delta DIC_{adv/rro}$. As the primary production is minimal in the dark season, the ΔC:ΔN ratio for January is most likely erroneous.

The annually integrated NCP estimates at the IsA Station are altogether quite modest in comparison to incubation-based NCP estimates of 85 g C m^{-2} yr^{-1} in the Godthåbsfjord in south-east Greenland (Meire et al. 2015) and 108 g C m^{-2} yr^{-1} in the Fram Strait–Svalbard region (Vaquer-Sunyer et al. 2013). A discrepancy between mass-balance NCP estimates and in situ incubation-based estimates has been acknowledged by a number of authors, including Codispoti et al. (2013). One explanation could be the different time scales of the methods, that is, seasonal changes versus instantaneous measurements.

Interannual variability: the links between water masses

Despite the fact that the NCP estimates to some extent reflect the chosen method, the biological CO_2 consumption during the productive season at the IsA Station was fairly high, although there were some differences between the years. The ArW had an earlier onset of the spring bloom compared to TAW, but the natural variability in the timing of the bloom is difficult to constrain with only three years of data. Hodal et al. (2012) showed that the bloom occurred between April and May in Kongsfjorden, for the years 2002, 2003, 2006 and 2007, which was similar to what we found in Adventfjorden.

The ΔC:ΔN uptake ratio was also estimated for the months of major productivity. The value for the IsA Station was 8.7 ± 0.6 when ArW was present as compared to 6.6 ± 0.5 when TAW was present (Table 2). This difference between water masses was also observed by Frigstad et al. (2014), who found seston C:N ratios of 7.9 and 6.7 for ArW and AW, respectively, in the Barents Sea. The drawdown of CO_2 at the IsA Station resulted in the seasonal NCP for ArW being nearly 20 g C m^{-2} higher than that of the TAW, as estimated from ΔDIC_{bio}. The high primary production of the ArW maximizes the TA:DIC ratio and CO_2 buffer capacity (the Revelle factor reaches a minimum of 11), which results in Ω_{Ar} of up to 2.4. On the other hand, the ArW also has the lowest TA:DIC ratio and CO_2 buffer capacity in winter with the Revelle factor close to 15 and Ω_{Ar} of 1.5. A high DIC content in the ArW of the CC was observed by Fransson et al. (2016), who suggested it to reflect sea-ice processes, especially in Storfjorden, in east Spitsbergen, where excessively high DIC content also has been observed (Omar et al. 2005). This will result in a low TA:DIC ratio.

Altogether, the seasonal differences in Ω_{Ar} are slightly larger for ArW (>0.8) as compared to those of TAW (about 0.7). Increased intrusions of TAW and/or AW into the fjord system in the future could possibly lower the NCP, with the potential to reduce the CO_2 buffer capacity and Ω_{Ar} over the summer season. In winter time, on the other hand, the presence of TAW/AW will contribute to a slightly higher CO_2 buffer capacity and Ω_{Ar} as opposed to the presence of colder and CO_2-enriched ArW.

Future outlook

The uptake of anthropogenic CO_2 will continue to lower the TA:DIC ratio, reduce the CO_2 buffer capacity of the surface water (increase the Revelle factor), as well as lower the pH and decrease $[CO_3^{2-}]$. For a yearly increase in pCO_2 of 1 µatm yr^{-1} because of anthropogenic CO_2 uptake, as observed in the WSC by Olsen et al. (2006),

Citation: *Polar Research* 2019, *38*, 3345, http://dx.doi.org/10.33265/polar.v38.3345

Ω_{Ar} of the TAW will decrease by −0.0036 yr^{-1} (when using a temperature of 2°C). This value would double for a yearly increase in pCO_2 of 2 µatm yr^{-1}. How severe the consequences will be for Ω depends on the fate of the absorbed anthropogenic CO_2, which is intricately linked to the future NCP. The melting of the Spitsbergen snow and glacial cap will have consequences not only for the stratification and mixing of the water column, but it will also change the light conditions/optical properties and biogeochemistry of the water through input of bedrock eroded minerals (e.g., carbonate- or silica-rich minerals; Fransson et al. 2015) and decaying organic materials. The fate of the NCP is ultimately dependent on how the marine ecosystems will respond to these climate change-induced changes. A next step to uncover these future uncertainties would be to resolve the sensitivity of the NCP to the timing of the bloom and the duration of the productive season in relation to the presence of either ArW or TAW and the onset of the melt season. For instance, does the occurrence of TAW in the fjord result in an earlier melt season and will an earlier melt season with a higher freshwater discharge—with subsequent reduction in water column light availability because of high sediment load—result in a shorter productive season and altogether lower NCP?

Acknowledgements

Data for this study are to be submitted to the Norwegian Marine Data Centre within one year after the publication. Until then, the data can be accessed from the corresponding author. Metadata are available at the Research in Svalbard Database portal (www.researchinsvalbard.no). The authors thank their colleagues at the Logistics Services and Arctic Biology Department at UNIS for their invaluable fieldwork support and help. Finally, they thank the Norwegian Meteorological Institute for the data from Svalbard Airport and the Norwegian Institute for Air Research, especially Cathrine Myhre Lund, Ove Hermansen and Paul Eckhardt, for the atmospheric CO_2 data that are available from the EBAS database (http://ebas.nilu.no). They also acknowledge the support from the Norwegian Research Council project Signals from the Arctic Ocean in the Atmosphere. The authors gratefully acknowledge the valuable comments and suggestions from two anonymous reviewers.

Disclosure statement

No potential conflict of interest was reported by the authors.

Funding

Funding for this study was provided by the Norwegian Research Council under an Arctic Field Grant (Research in Svalbard Database nos. 10127; 10404; 10662), with additional fieldwork support from UNIS and the Ocean Acidification flagship programme at the FRAM—High North Centre for Climate and the Environment, Norway, to AF and MC.

References

Alpkem 1989. Nitrate+nitrite nitrogen. *A303-S170. Revision 6–89. RFA (rapid flow analyser) methodology.* College Station, TX: Alpkem.

Bendschneider K. & Robinson R.I. 1952. A new spectrophotometric method for determination of nitrite in seawater. *Journal of Marine Research 2*, 87–96.

Chen B., Cai W.-J. & Chen L. 2015. The marine carbonate system of the Arctic Ocean: assessment of internal consistency and sampling considerations, summer 2010. *Marine Chemistry 176*, 174–188, http://dx.doi.org/10.1016/j.marchem.2015.09.007.

Chierici M., Fransson A. & Anderson L.G. 1999. Influence of m-cresol purple indicator additions on the pH of seawater samples: correction factors evaluated from a chemical speciation model. *Marine Chemistry 65*, 281–290, http://dx.doi.org/10.1016/S0304-4203(99)00020-1.

Chierici M., Fransson A., Lansard B., Miller L.A., Mucci A., Shadwick E., Thomas H., Tremblay J.E. & Papakyriakou T.N. 2011. The impact of biogeochemical processes and environmental factors on the calcium carbonate saturation state in the Circumpolar Flaw Lead in the Amundsen Gulf, Arctic Ocean. *Journal of Geophysical Research—Oceans 116*, C00G09, http://dx.doi.org/10.1029/2011JC007184.

Clayton T.D. & Byrne R.H. 1993. Spectrophotometric seawater pH measurements: total hydrogen ion concentration scale calibration of m-cresol purple and at-sea results. *Deep-Sea Research Part I 40*, 2115–2129, http://dx.doi.org/10.1016/0967-0637(93)90048-8.

Codispoti L.A., Kelly V., Thessen A., Matrai P., Suttles S., Hill V., Steele M. & Light B. 2013. Synthesis of primary production in the Arctic Ocean: III. Nitrate and phosphate based estimates of net community production. *Progress in Oceanography 110*, 126–150. http://dx.doi.org/10.1016/j.pocean.2012.11.006.

Cottier F.R., Tverberg V., Inall M.E., Svendsen H., Nilsen F. & Griffiths C. 2005. Water mass modification in an Arctic fjord through crossshelf exchange: the seasonal hydrography of Kongsfjorden, Svalbard. *Journal of Geophysical Research—Oceans 110*, C12005, http://dx.doi.org/10.1029/2004JC002757.

Dickson A.G. 1990. Standard potential of the reaction: AgCl(s) + 1/2H2 (g) = Ag(s) + HCl(aq), and the standard acidity constant of the ion HSO_4^- in synthetic sea water from 273.15 to 318.15 K. *Journal of Chemical Thermodynamics 22*, 113–127, http://dx.doi.org/10.1016/0021-9614(90)90074-Z.

Dickson A.G. & Goyet C. (eds.) 1994. *Handbook of methods for the analysis of the various parameters of the carbon dioxide system in sea water, version 2. ORNL/CDIAC-74*. Oak Ridge, TN: Carbon Dioxide Information Analysis Center, Oak Ridge National Laboratory, US Department of Energy.

Dickson A.G. & Millero F.J. 1987. A comparison of the equilibrium constants for the dissociation of carbonic acid in seawater media. *Deep-Sea Research Part A 34*, 1733–1743, http://dx.doi.org/10.1016/0198-0149(87)90021-5.

Dickson A.G., Sabine C.L. & Christian J.R. (eds.) 2007. *Guide to best practices for ocean CO_2 measurements. PICES Special Publication 3. IOCCP Report 8.* Sidney, Canada: North Pacific Marine Science Organization.

Doney S.C., Balch W.M., Fabry V.J. & Feely R.A. 2009. Ocean acidification: a critical emerging problem for the ocean sciences. *Oceanography 22*, 16–25, http://dx.doi.org/10.5670/oceanog.2009.93.

Ericson Y., Falck E., Chierici M., Fransson A., Kristiansen S., Platt S.M., Hermansen O. & Myhre C.L. 2018. Temporal variability in surface water pCO_2 in Adventfjorden (west Spitsbergen) with emphasis on physical and biogeochemical drivers. *Journal of Geophysical Research—Oceans 123*, 4888–4905, http://dx.doi.org/10.1029/2018JC014073.

Ewertowski M. 2014. Recent transformations in the High-Arctic glacier landsystem, Ragnabreen, Svalbard. *Geografiska Annaler Series A 96*, 265–285, http://dx.doi.org/10.1111/geoa.12049.

Fransson A., Chierici M., Hop H., Findlay H.S., Kristiansen S. & Wold A. 2016. Late winter-to-summer change in ocean acidification state in Kongsfjorden, with implications for calcifying organisms. *Polar Biology 39*, 1841–1857, http://dx.doi.org/10.1007/s00300-016-1955-5.

Fransson A., Chierici M., Nomura D., Granskog M.A., Kristiansen S., Martma T. & Nehrke G. 2015. Effect of glacial drainage water on the CO_2 system and ocean acidification state in an Arctic tidewater-glacier fjord during two contrasting years. *Journal of Geophysical Research—Oceans 120*, 2413–2429, http://dx.doi.org/10.1002/2014JC010320.

Frigstad H., Andersen T., Bellerby R.G.J. Silyakova A. & Hessen D.O. 2014. Variation in the seston C:N ratio of the Arctic Ocean and pan-Arctic shelves. *Journal of Marine Systems 129*, 214–223, http://dx.doi.org/10.1016/j.jmarsys.2013.06.004.

Grabiec M. Ignatiuk D., Jania J.A., Moskalik M., Glowacki P., Blaszczyk M., Budzik T. & Walczowski W. 2017. Coast formation in an Arctic area due to glacier surge and retreat: the Hornbreen–Hambergbreen case from Spistbergen. *Earth Surface Processes and Landforms 43*, 387–400, http://dx.doi.org/10.1002/esp.4251.

Grasshof K. 1965. *On the automatic determination of phosphate, silicate and fluoride in seawater. ICES Hydrographic Committee Report 129.* Copenhagen: International Council for the Exploration of the Sea.

Grasshof K., Kremling K. & Ehrhardt M. 2009. *Methods of seawater analysis*. 3rd edn. New York: John Wiley.

Hodal H., Falck-Petersen S., Hop H., Kristiansen S. & Reigstad M. 2012. Spring bloom dynamics in Kongsfjorden, Svalbard: nutrients, phytoplankton, protozoans and primary production. *Polar Biology 35*, 191–203, http://dx.doi.org/10.1007/s00300-011-1053-7.

Isaksen K., Nordli Ø., Førland E. J., Lupikasza E., Eastwood S. & Niedźwiedź T. 2016. Recent warming on Spitsbergen—influence of the atmospheric circulation and sea ice cover. *Journal of Geophysical Research—Atmospheres 121*, 11913–11931, http://dx.doi.org/10.1002/2016JD025606.

Kähler P. & Koeve W. 2001. Marine dissolved organic matter: can its C:N ratio explain carbon overconsumption? *Deep-Sea Research Part I 48*, 49–62, http://dx.doi.org/10.1016/S0967-0637(00)00034-0.

Lee K., Kim T.-W., Byrne R.H., Millero F.J., Feely R.A. & Liu Y.-M. 2010. The universal ratio of boron to chlorinity for the North Pacific and North Atlantic oceans. *Geochimica et Cosmochimica Acta 74*, 1801–1811, http://dx.doi.org/10.1016/j.gca.2009.12.027.

Lewis E. & Wallace D.W.R. 1998. Program developed for CO_2 system calculations. *ORNL/CDIAC-105. Oak Ridge, TN: Carbon Dioxide Information Analysis Center, Oak Ridge National Laboratory*, US Department of Energy.

Lydersen C., Assmy P., Falk-Petersen S., Kohler J., Kovacs K.M., Reigstad M., Steen H., Strøm H., Sundfjord A., Varpe Ø., Walczowski W., Weslawski J.M. & Zajaczkowski M. 2014. The importance of tidewater glaciers for marine mammals and seabirds in Svalbard, Norway. *Journal of Marine Systems 129*, 452–471, http://dx.doi.org/10.1016/j.jmarsys.2013.09.006.

Marlin C., Tolle F., Griselin M., Bernard E., Saintenoy A., Quenet M. & Friedt J.-M. 2017. Change in geometry of a High Arctic glacier from 1948 to 2013 (Austre Lovénbreen, Svalbard). *Geografiska Annaler Series A 99*, 115–138, http://dx.doi.org/10.1080/04353676.2017.1285203.

Marquardt M., Vader A., Stübner E.I., Reigstad M. & Gabrielsen T.M. 2016. Strong seasonality of marine microbial eukaryotes in a High-Arctic fjord (Isfjorden, in west Spitsbergen, Norway). *Applied and Environmental Microbiology 82*, 1868–1880, http://dx.doi.org/10.1128/AEM.03208-15.

Mehrbach C., Culberson C.H., Hawley J.E. & Pytkowicz R.M. 1973. Measurement of the apparent dissociation constants of carbonic acid in seawater at atmospheric pressure. *Limnology and Oceanography 18*, 897–907, http://dx.doi.org/10.4319/lo.1973.18.6.0897.

Meire L., Søgaard D.H., Mortensen J., Meysman F.J.R., Soetaert K., Arendt K.E., Juul-Pedersen T., Blicher M.E. & Rhysgaard S. 2015. Glacial meltwater and primary production are drivers of strong CO_2 uptake in fjord and coastal waters adjacent to the Greenland Ice Sheet. *Biogeosciences 12*, 2347–2363, http://dx.doi.org/10.5194/bg-12-2347-2015.

Millero F.J. 1979. The thermodynamics of the carbonate system in seawater. *Geochimica et Cosmochimica Acta 43*, 1651–1661, http://dx.doi.org/10.1016/0016-7037(79)90184-4.

Millero F.J. 2007. The marine inorganic carbon cycle. *Chemical Reviews 107*, 308–341, http://dx.doi.org/10.1021/cr0503557.

Mucci A. 1983. The solubility of calcite and aragonite in seawater at various salinities, temperatures, and one

atmosphere total pressure. *American Journal of Science 283*, 780–799, http://dx.doi.org/10.2475/ajs.283.7.780.

Muckenhuber S., Nilsen F., Korosov A. & Sandven S. 2016. Sea ice cover in Isfjorden and Hornsund, Svalbard (2000–2014) from remote sensing data. *The Cryosphere 10*, 149–158, http://dx.doi.org/10.5194/tc-10-149-2016.

Nilsen F., Cottier F., Skogseth R. & Mattsson S. 2008. Fjord–shelf exchanges controlled by ice and brine production: the interannual variation of Atlantic Water in Isfjorden, Svalbard. *Continental Shelf Research 28*, 1838–1853, https://doi.org/10.1016/j.csr.2008.04.015.

Nilsen F., Skogseth R., Vaardal-Lunde J. & Inall M. 2016. A simple shelf circulation model: Intrusion of Atlantic Water on the West Spitsbergen Shelf. *Journal of Physical Oceanography 46*, 1209–1230. http://dx.doi.org/10.1175/JPO-D-15-0058.1.

Nordli Ø., Przybylak R., Ogilvie A.E.J. & Isaksen K. 2014. Long-term temperature trends and variability on Spitsbergen: the extended Svalbard Airport temperature series, 1898–2012. *Polar Research 33*, article no. 21349, http://dx.doi.org/10.3402/polar.v33.21349.

Olsen A., Omar A.M., Bellerby R.G.J., Johannessen T., Ninnemann U., Brown K.R., Olsson K.A., Olafsson J., Nondal G., Kivimäe C., Kringstad S., Neill C. & Olafsdottir S. 2006. Magnitude and origin of the anthropogenic CO_2 increase and ^{13}C Suess effect in the Nordic seas since 1981. *Global Biogeochemical Cycles 20*, GB3027, http://dx.doi.org/10.1029/2005GB002669.

Omar A., Johannessen T., Bellerby R.G.J., Olsen A., Anderson L.G. & Kivimäe C. 2005. Sea ice and brine formation in Storfjorden: implications for the Arctic winter time air–sea CO_2 flux. In H. Drange et al . (eds.): *The Nordic seas: an integrated perspective.* Pp. 177–187. Washington, DC: American Geophysical Union.

Onarheim I.H., Smedsrud L.H., Ingvaldsen R.B. & Nilsen F. 2014. Loss of sea ice during winter north of Svalbard. *Tellus Series A 66*, article no. 23933, http://dx.doi.org/10.3402/tellusa.v66.23933.

Pavlov A.K., Tverberg V., Ivanov B.V., Nilsen F., Falk-Petersen S. & Granskog M.A. 2013. Warming of Atlantic Water in two west Spitsbergen fjords over the last century (1912–2009). *Polar Research 32*, article no. 11206, http://dx.doi.org/10.3402/polar.v32i0.11206.

Redfield A.C., Ketchum B.H. & Richards F.A. 1963. The influence of organisms on the composition of sea-water. In M.N. Hill (ed.): *The sea: ideas and observations on the progress in the study of the sea. Vol. 2*. Pp. 26–77. New York: Interscience.

Riley J.P. & Tongudai M. 1967. The major cation/chlorinity ratios in sea water. *Chemical Geology 2*, 263–269.

Sarmiento J.L. & Gruber N. 2006. *Ocean biogeochemical dynamics*. Princeton, NJ: Princeton University Press.

Shadwick E.H., Thomas H., Chierici M., Else B., Fransson A., Michel C., Miller L.A., Mucci A., Niemi A., Papakyriakou T.N. & Tremblay J.-E. 2011. Seasonal variability of the organic carbon system in the Amundsen Gulf region of the southeastern Beaufort Sea. *Limnology and Oceanography 56*, 303–322.

Sobota I. & Nowak M. 2014. Changes in the dynamics and thermal regime of the permafrost and active layer of the High Arctic coastal area in north-west Spitsbergen, Svalbard. *Geografiska Annaler Series A 96*, 227–240, http://dx.doi.org/10.1111/geoa.12045.

Sterner R.W., Andersen T., Elser J.J., Hessen D.O., Hood J.M., McCauley E., Urabe J. 2008. Scale-dependent carbon:nitrogen:phosphorus seston stoichiometry in marine and freshwaters. *Limnology and Oceanography 53*, 1169–1180, http://dx.doi.org/10.4319/lo.2008.53.3.1169.

Takahashi T., Olafsson J., Goddard J.G., Chipman D.W. & Sutherland S.C. 1993. Seasonal variation of CO_2 and nutrients in the high latitude surface oceans: a comparative study. *Global Biogeochemical Cycles 7*, 843–878, http://dx.doi.org/10.1029/93GB02263.

van Heuven S., Pierrot D., Rae J.W.B., Lewis E. & Wallace D.W.R. 2011. *MATLAB program developed for CO_2 system calculations. ORNL/CDIAC-105b.* https://doi.org/10.3334/CDIAC/otg.CO_2SYS_MATLAB_v1.1. Oak Ridge, TN: Carbon Dioxide Information Analysis Center, Oak Ridge National Laboratory, US Department of Energy.

Vaquer-Sunyer R., Duarte C.M., Regaudie-de-Gioux A., Holding J. Garcia-Corral L.S., Reigstad M. & Wassman P. 2013. Seasonal patterns in Arctic planktonic metabolism (Fram Strait–Svalbard region). *Biogeosciences 10*, 1451–1469, http://dx.doi.org/10.5194/bg-10-1451-2013.

Wanninkhof R. 2014. Relationship between wind speed and gas exchange over the ocean revisited. *Limnology and Oceanography—Methods 12*, 351–362, http://dx.doi.org/10.4319/lom.2014.12.351.

Weiss R.F. 1974. Carbon dioxide in water and seawater: the solubility of a non-ideal gas. *Marine Chemistry 2*, 203–205, http://dx.doi.org/10.1016/0304-4203(74)90015-2.

WMO 2014. *Guide to meteorological instruments and methods of observation. WMO-No 8.* Geneva: World Meteorological Organization.

Woosley R.J., Millero F.J. & Takahashi T. 2017. Internal consistency of the inorganic carbon system in the Arctic Ocean. *Limnology and Oceanography—Methods 15*, 887–896, https://dx.doi.org/10.1002/lom3.10208.

Ziaja W. 2005. Response of the Nordenskiöld Land (Spitsbergen) glaciers Grumantbreen, Håbergbreen and Dryadbreen to the climate warming after the Little Ice Age. *Annals of Glaciology 42*, 189–194, http://dx.doi.org/10.3189/172756405781812673.